



Efficiently Writing Bragg Grating in High-Birefringence Elliptical Microfiber for Label-Free Immunosensing with Temperature Compensation

Peng Xiao^{1,2} · Zhiyuan Xu¹ · Deming Hu¹ · Lili Liang^{1,3} · Lipeng Sun¹ · Jie Li¹ · Yang Ran¹ · Bai-Ou Guan¹

Received: 5 December 2020 / Accepted: 8 June 2021 / Published online: 30 June 2021
© Donghua University, Shanghai, China 2021

Abstract

Immunosensor is a powerful tool in healthcare and clinic, food and drug industry, and environmental protection. Label-free fiber-optic immunosensors have shown a myriad of advantages, such as high sensitivity, anti-electromagnetic interference, and afield measurement via the fiber network. However, the fiber-optic based sensor may bear the temperature cross-talk, especially under the warming condition for bio-activating the immune molecules. In this study, we proposed a highly birefringent microfiber Bragg grating for immunosensing with the temperature-compensation. The birefringent microfiber was drawn from the elliptical cladding multimode fiber that was ablated by the CO₂ laser. The considerably large energy overlap region offered by the original multimode fiber favored the efficient inscription of FBG with high reflectivity. The dual resonances derived by the orthogonal polarization states presented similar temperature responsivities but significantly different ambient refractive index sensitivities, allowing the temperature-compensational RI sensing. The human immunoglobulin G (IgG) molecules were anchored on the surface of the microfiber grating probe by the covalent functionalization technique to enable the specific detection of the anti-IgG molecule. The proposed method promises a high-efficiency and low-cost design for the microfiber Bragg grating-based biosensor without being subjected to the temperature cross-sensitivity.

Keywords Fiber-optic biosensors · Microfiber · Fiber Bragg grating · Birefringence · Temperature compensation · Immunosensing

Introduction

The past several decades have witnessed the robust and rapid development of fiber optic sensors, which have gained outstanding reputations regarding their advantages, such as ease of fabrication, high sensitivity, resistance to electromagnetic interference, and remote sensing capability. Among their peers, the fiber optic refractive-index sensors have emerged

as a promising analytical tool for detecting biomolecules and therefore facilitating disease diagnosis [1–11]. Myriads of fiber optic refractive-index sensing strategies have been successfully implemented into the biosensors, including fiber interferometry [12–16], fiber gratings [17–22], fiber resonators [23–26], fiber surface plasmonic resonance [27–30], and fiber optofluidics [31–34]. As one of the most reliable and commercialized fiber optic sensors, fiber Bragg grating outweighs its counterparts in intrinsic reflective operation, compact footprint, and sharp signal bandwidth that enables high-resolution interrogation and multiplexing. It is yet conventionally excluded by the RI sensing implementations due to the barricade of fiber cladding that blocks the transverse energy from spreading out to the ambient. The microfiber Bragg grating (μ FBG) has enabled an excellent platform that can overcome the limitation. The microfiber offers not only the structural flexibility lying in the extreme curvature tolerance but also a large evanescent wave that allows the high ambient RI responsivity of Bragg grating written on it,

✉ Yang Ran
tranyang@jnu.edu.cn

✉ Bai-Ou Guan
tguanbo@jnu.edu.cn

¹ Guangdong Provincial Key Laboratory of Optical Fiber Sensing and Communications, Institute of Photonics Technology, Jinan University, Guangzhou 510632, China

² Ji Hua Laboratory, Foshan 528300, China

³ Institute of Information Technology, Handan University, Handan 056005, China

opening a new pathway for the realization of the fiber Bragg grating-based biosensors [35–42].

However, the temperature cross-talk due to the thermo-optic effect may affect the accuracy of the measurement using microfiber Bragg grating biosensors, in which the test would be carried out under warming conditions for maintaining the activity of the bio-molecules. Routine methods mainly adopt the cascaded or paralleled sensing elements that one acts as the sensor for measurand, and another plays the role of reference. Sun et al. had reported an FBG-assisted tapered fiber interferometer that achieved the temperature-insensitive breast cancer indicated protein sensing [43]. Cao et al. demonstrated a microwave frequency domain interrogated μ FBG breast cancer biomarker sensor that involved an additional FBG as the temperature compensator [44]. Nevertheless, the enrollment of the additional temperature referral would inevitably compromise the compactness and simplicity of the sensor scheme. Deeply exploring more degrees of freedom of the signal from just one μ FBG scheme for the temperature-compensational sensing is a feasible way to address the problem.

Several additional-device-free options have shown for the rule-out of the temperature cross-sensitivity, utilizing the multiple resonances of the μ FBG. The difference between the resonances lies in the transverse modes [45–47], harmonic orders [48], and polarization states [49]. The polarization states deriving dual-resonance scheme has a closer wavelength-space attributed to the fiber birefringence, highly reducing the demodulating range of the wavelengths. Therefore, the low-cost demodulation instrument could be employed. Furthermore, the dual-polarized resonances scheme can also be compatible with the other two techniques, which would favor the demands for multiple measurands sensing. However, the demonstrated birefringent μ FBG so far has encountered several hindrances. First, the rectangular cladding fiber, drawn by the special method, would inevitably increase the fabrication cost and result in incompatibility with the conventional fiber-transmission system. Second, the rectangular cladding fiber has a similar core structure to the single-mode fiber that is not photosensitive as is tapered into microfiber. The efficiency of the inscription is low. Third, due to the tiny overlap integral region under the ultraviolet light modulation, the reflectivity of the Bragg grating is normally limited, suffering the annihilation if the bilayer coating is involved on the fiber surface.

In this paper, we have proposed an efficient method to fabricate the highly birefringent (Hi-Bi) microfiber Bragg grating (μ FBG) and demonstrated its utility of temperature-compensational biosensing. The elliptical cladding fiber was ablatively fabricated through the irradiation of the CO_2 laser on the conventional multimode telecom fiber. By tuning the intensity of the CO_2 laser, the ellipticity of the fiber cladding could be engineered that is essential for enabling the

birefringence as the fiber was thinned to several microns in diameter. The considerably large core region offered by the original multimode fiber allowed the rapid inscription of FBG on it, in which the grating strength was guaranteed. After characterizing the response curve regarding the ambient refractive index (RI) and temperature, the Hi-Bi μ FBG has featured the temperature compensation capability in RI sensing. Finally, the immunosensor based on the Hi-Bi μ FBG was developed through the covalent functionalization method for the highly specific detection of human anti-IgG.

Experimental Section

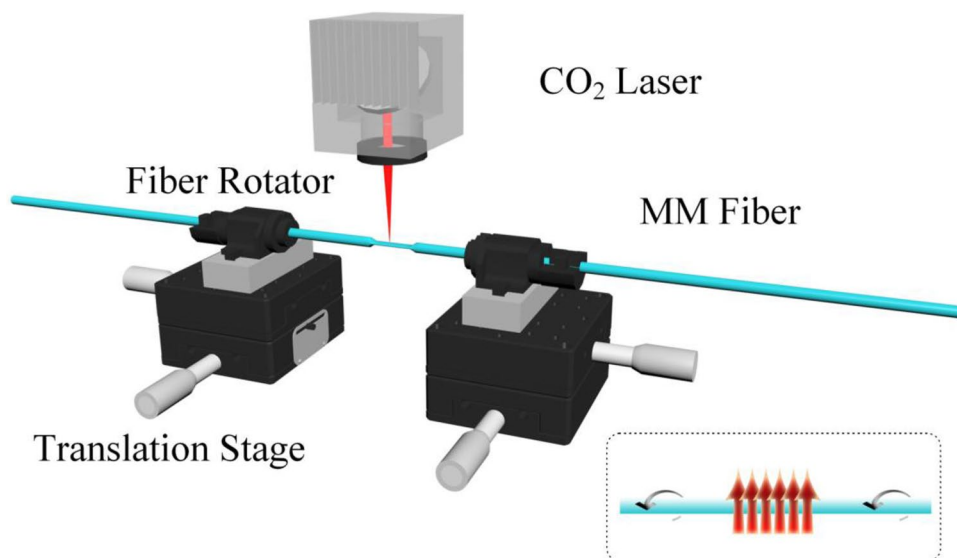
Materials

The optical fiber used is the telecom multimode (62.5/125) silica fibers, which was purchased from Corning Inc. (USA). Sulfuric acid, hydrogen peroxide, pure ethanol, phosphate buffered saline (PBS), 25% glutaraldehyde water solution, bull serum albumin (BSA) were obtained from Sangon Biotech (Shanghai, China). 99% 3-aminopropyltriethoxysilane (APTES) was purchased from Sigma-Aldrich (Darmstadt, Germany). Human immunoglobulin G protein (IgG) and mouse anti-IgG monoclonal antibody were bought from Sino Biological Inc. (China). All the chemicals and biological materials were of analytical grade. Deionized (DI) water was used throughout the experiment.

Preparation of the Elliptical Fiber

The previous report had adopted the femtosecond laser machining method to facilitate high-precision shaping of the silica cladding of the fiber [50]. In this work, our strategy utilized the fast scanning CO_2 laser ablation approach for high-efficiently fabricating the elliptical fiber from the standard cylindrical fiber. Figure 1 presents a schematic diagram of the fiber CO_2 laser ablation method. A pulsed CO_2 laser (SYNRAD 48) with a wavelength of 10.6 μm and a maximum output power of 50 W was integrated into the system as the ablation source. The laser beam was focused into a spot of a diameter of 50 μm by a build-in ZnSe lens. The parameters of the laser, such as the output power, scanning path and speed, and the number of scanning cycles, could be flexibly configurated and precisely controlled by the computer. In this experiment, the scanning speed and repetition frequency were set to 300 mm/s and 1000 Hz, respectively. The scanning paths were parallelly distributed, but the scanning direction was vertical to the fiber axis, as shown in the inset of Fig. 1. The ablation length of the fiber was about 6 mm. After a 5-s ablation, the cladding of one side was partly removed. Then the fiber was axially rotated by 180° to conduct another 5-s ablation on the other side of

Fig. 1 Scheme of the elliptical fiber fabrication using the CO₂ laser ablation. *MM fiber* multimode fiber



the fiber. The entire process was monitored by a CCD camera for obtaining the ablation status of the fiber in real-time. Due to the absorption distribution of the cladding to the CO₂ laser ablation in the vertical direction, the fiber possessed an elliptical cladding profile in the cross-section.

Preparation of the Elliptical Microfiber Bragg Grating

To facilitate the Bragg grating inscription on the elliptical microfiber, the standard multimode fiber (62.5/125 from Corning, Ltd) was employed as the preliminary fiber in the experiment. The ovalized cladding multimode fiber can maintain the photosensitivity as it was tapered to the elliptical microfiber [51, 52]. The elliptical microfiber was tapered by the flame-heated drawing technique, as shown in Fig. 2a.

The fast tapering method (< 10 s) was adopted to minimize the core expansion effect. The thinned core allowed the spread of the transverse modes into the ovalized cladding that enabled a significant geometrical birefringence. Moreover, the abrupt cone region of microfiber induced by the fast tapering process may excite lower order modes into the grating coupling, resulting in more valuable resonances that provide additional signals for measurements [45, 51]. As shown in Fig. 2b, a homemade FBG inscription system involving a 193 nm ArF ultraviolet (UV) excimer laser (BraggStar Industrial, Coherent, USA) and a phase mask (Ibsen, Denmark) with a pitch of 1072.15 nm was utilized to inscribe the Bragg grating into the microfiber. The repetition rate of the laser was set to 200 Hz. The UV energy density was set to 120 mJ/cm² per pulse through a cylindrical lens (Thorlabs, USA). The UV-laser output was spatially immobilized and

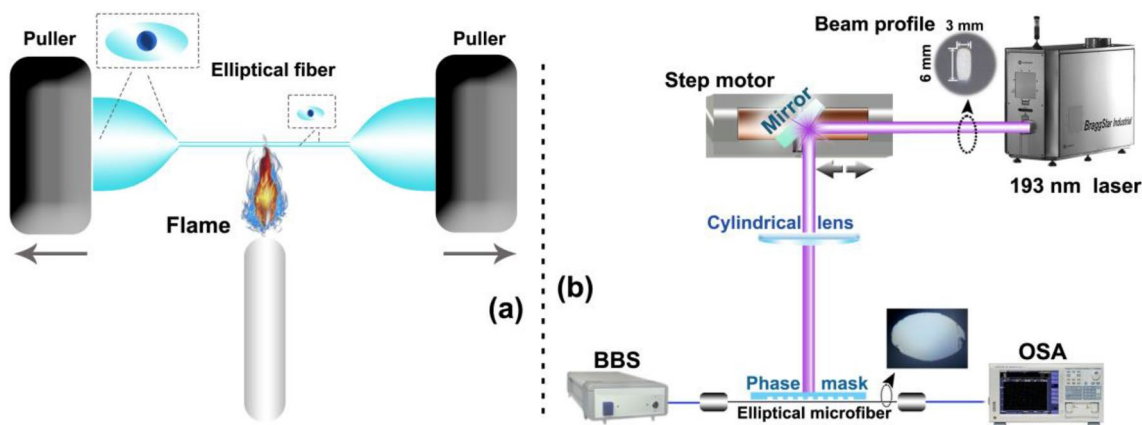


Fig. 2 a Flame-drawn method for preparing the elliptical microfiber; b scheme of elliptical microfiber Bragg grating inscription. *BBS* broadband source, *OSA* optical spectrum analyzer

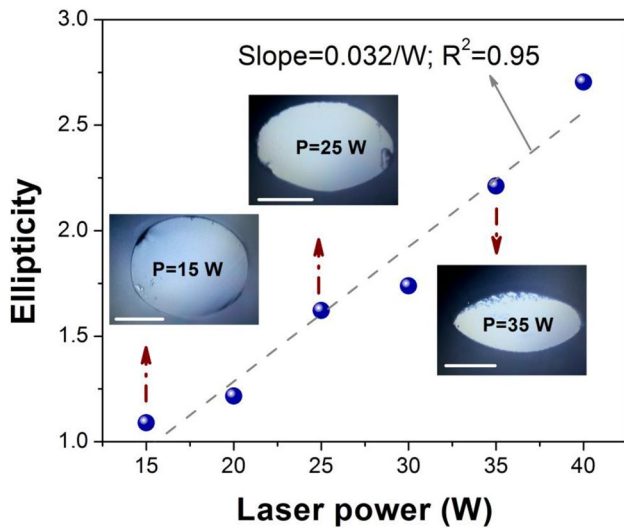


Fig. 3 Ellipticity of the fiber corresponding to the intensity CO₂ laser in the ablation. Insets: the microscopic images of cross section of the elliptical fiber. Scales bars indicate the length of 50 μm

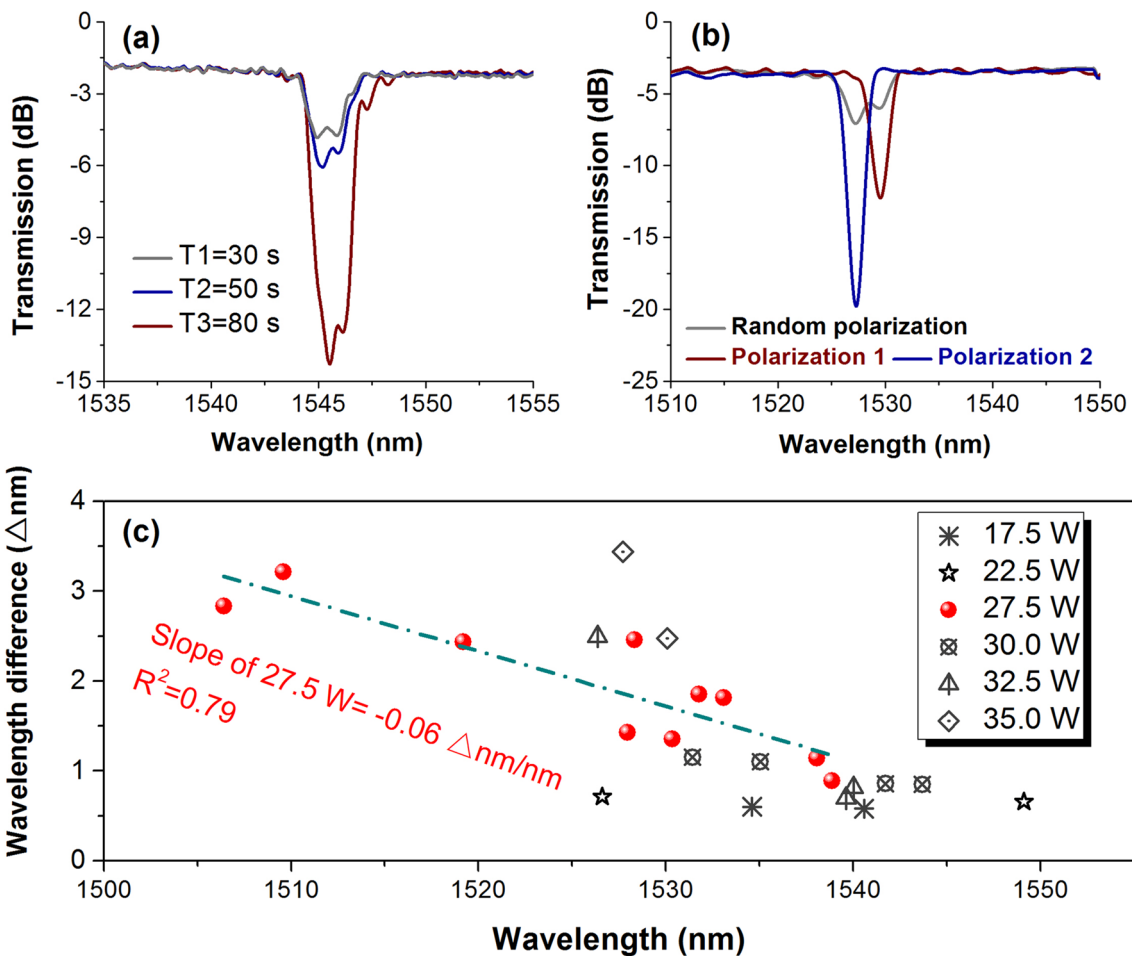


Fig. 4 **a** Spectral evolution of a highly birefringent microfiber Bragg grating ($D=5\ \mu\text{m}$); **b** polarization dependence of the resonances of the 3 μm -fiber Bragg grating ($D=3\ \mu\text{m}$); **c** dependence of the wave-

length difference mediated by the birefringence of the elliptical microfiber to the transverse size and CO₂ laser ablating power

focused on the uniform waist of the microfiber. The grating length was determined by the width of the laser beam ($\sim 3\ \text{mm}$). A broadband LED source (BBS, GoLight, China) with a wavelength range of 1250–1650 nm and an average power density of $\sim 20\ \text{dBm/nm}$ was connected to one end of the microfiber for offering the background light reference. An optical spectrum analyzer (OSA, AQ6370D, Yokogawa, Japan), which was linked to another end of the microfiber, was serving with a resolution of 0.01 nm for logging the transmission spectrum of the elliptical microfiber Bragg grating.

Results and Discussion

Characterization of the Hi-Bi Microfiber Bragg Gratings

By adjusting the power of the CO₂ laser output, the cross profile of the fiber with regard to the laser power is

illustrated in Fig. 3. A more intense laser output would result in a more significant ellipticity of the fiber. The dependence between the ellipticity and the laser followed a linear correlation with a slope of 0.032 per Watt. The ellipticity derived the birefringence of the microfiber, which was tapered from the elliptical fiber [53]. It reveals that the birefringence of the microfiber could be flexibly tuned through setting the proper laser output power.

Figure 4a depicts the evolution of the Bragg grating on a 5 μm (the length of the longer axial of the ellipse cross-section) microfiber with the cross ellipticity of 1.6 during the inscription. The grating resonance with a dual-dip spectrum went deeper as the fluence accumulating. The dips at longer and shorter wavelengths were inherited by the longer and shorter axial lengths of the ellipse, respectively. The wavelength difference of the two dips associated to the orthogonal polarization states was about 0.7 nm, indicating a birefringence of 6×10^{-4} by the elliptical microfiber. The grating with a strength of 13 dB ($\sim 95\%$) could be obtained by consuming only 80 s of laser inscription. It was noted that the closer wavelengths of the dips enabled the overlap of the strength as the polarization state was not rigorously regulated, leading to an overall stronger resonance. However, if the wavelength of the dual dips was separated enough using the highly birefringent fiber, which eliminated the possibility of the strength overlapping, the two dips would not exceed 3 dB (50%) because the Bragg grating could reflect only one polarization state at each wavelength.

In the following, a microfiber with the same ellipticity of 1.6 but with a thinner size of 3 μm was prepared. It can be observed in Fig. 4b that, besides the blue shift of the resonances due to the thinner fiber, a larger wavelength difference of 2.3 nm was shown in the spectrum, inferring a birefringence of 2×10^{-3} . By adjusting the polarization state of the propagating light via a polarizer (Thorlabs, USA) and polarization controller (PC, Thorlabs, USA), each orthogonal polarization states could be strictly calibrated and facilitated the clear appearances of each polarized resonance. From the spectra, the resonances of polarization state 1 (longer wavelength dip) and polarization state 2 (shorter wavelength dip) achieved 10 dB (90%) and 15 dB (97%), presenting excellent reflectivity in both polarization directions. The results not only validated the description on the strength of highly birefringent fiber Bragg grating above but inferred that the birefringence of the elliptical microfiber could also be tuned through manipulating the transverse size of the microfiber in addition to the CO_2 laser ablating power.

Then, we elaboratively investigated the dependence of the birefringence of the elliptical microfiber, referring to the transverse size and CO_2 laser ablating power using the microfiber Bragg gratings. The results were shown in Fig. 4c. Here, the size (longer axis of the ellipse) of fiber

and the birefringence could be derived by the wavelength (x-coordinate) and the wavelength difference of the dual dips (y-coordinate), respectively. The birefringence of the microfiber using different ablating power revealed the reverse tendency to the size of the fiber. The thinner elliptical fiber possessed the larger geometrical birefringence. The higher ablation power rendered a higher slope between the resonant wavelength (indicating the fiber diameter) and the wavelength difference (indicating the fiber birefringence). However, higher ablation may also increase the fragility of the fiber when it was tapered, resulting in the higher bias of the fabrication. The lower ablation would weaken the birefringent effect. By considering either the fabrication bias and the birefringence effect, the 27.5 W ablating power of CO_2 laser was optimally preferred. The correlation between the transverse size and birefringence exhibited a quasi-linear curve, facilitating the reliability of the sensor preparation for the subsequent experiments. The results shown here also validated that the ellipticity of the fiber could be maintained referring to the birefringence of the microfiber that represented by the dual wavelength difference of the resonances.

Configuration of Hi-Bi Microfiber Bragg Grating Sensor

According to the parameter optimization, the CO_2 laser that was operated at the output of 27.5 W was used to ovalize the multimode fiber. The elliptical multimode fiber was then tapered to about 3 μm in size. The reflection spectrum was used for enabling the Hi-Bi μFBG to be a reflective probe for the measurement of the bio-analytes, shown in Fig. 5a. The Hi-Bi μFBG was connected by an optical circulator (Thorlabs, USA) that ruled the unidirectional transmission of the input light source. Thus, the reflection spectrum of the Hi-Bi μFBG could be monitored by the OSA. A PC and a polarizer functioned as the regulator of the polarization state of the transmitting light. After the Bragg grating inscription, the reflection spectrum of Hi-Bi μFBG was depicted in Fig. 5b. The dual-peak spectrum at ~ 1520 nm represented the Bragg resonances attributed to orthogonal polarization states of the fundamental mode. The wavelength difference between the two peaks was 2.05 nm, indicating the birefringence of microfiber was 1.9×10^{-3} . In addition to the fundamental resonances, a dual-peak spectrum at ~ 1490 nm with a larger wavelength difference of 2.3 nm was observed. The shorter dual peaks were generated by the coupling between the higher-order mode (HE_{21}) and fundamental mode (HE_{11}) [48, 51], referring to the two orthogonal polarization states either.

At first, the ambient refractive index (RI), which was the key mediator for the immunosensing was set as the measurand of the Hi-Bi μFBG sensor. The calibration solutions of RI indicators were prepared by using a mix of deionized

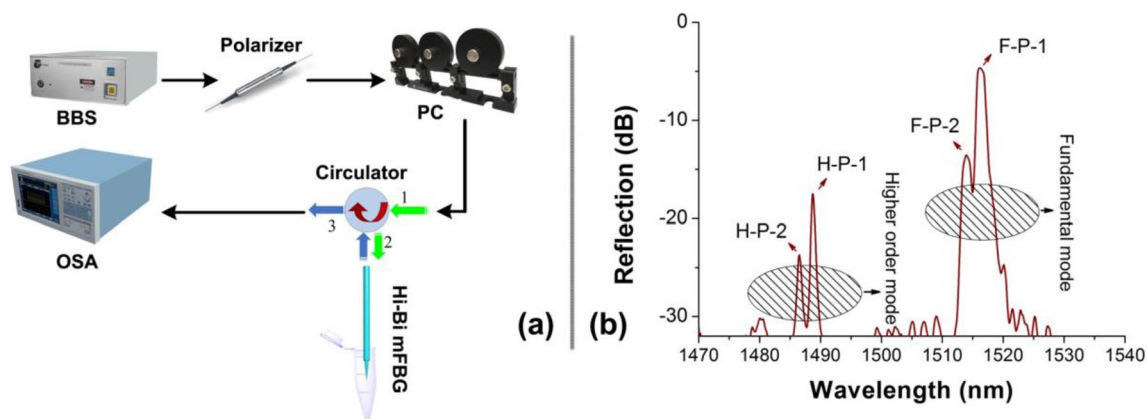


Fig. 5 **a** Scheme of the sensing experiment; **b** reflection spectrum of the Hi-Bi μ FBG. *PC* polarization controller, *BBS* broad-band source, *OSA* optical spectrum analyzer. “X-P-j” labels the resonance of the

grating (X: mode order; P-j: polarization state; F-P-1 means the “Fundamental mode Polarization-1”)

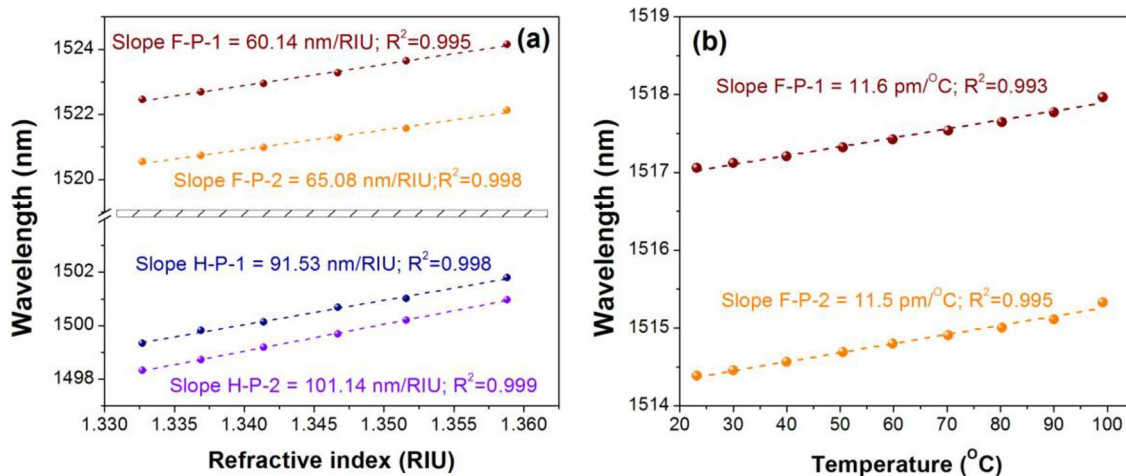


Fig. 6 Response curves of the Hi-Bi μ FBG with regard to **a** ambient refractive index; **b** temperature

water and ethanol. The RI value could be tuned ranging from 1.333 to 1.360 through altering the volume ratio of the two liquids and calibrated by a hand-held refractometer (PAL-RI, ATAGO, Japan). After recording the peak wavelengths of those resonances above-mentioned, the calibration curve could be plotted, which is shown in Fig. 6a. According to the plotting, higher-order mode resonances exhibited higher RI sensitivity (91.5 nm/RIU for H-P-1 and 101.14 nm/RIU for H-P-2) due to the outer distribution of the modal energy, which enabled a stronger evanescent wave at the interface between the silica fiber and the ambient solution. Meanwhile, the stronger evanescent wave also rendered a more significant divergence of the RI sensitivity between the two polarized resonances of the higher-order mode coupling. For the fundamental mode resonances, F-P-1 and F-P-2 presented the linear-responsivity of 60.1 and 65.0 nm/RIU. The sensitivities were lower than the higher-order

resonances, although, the stability after coating and the wavelength-distance away from the hydroxyl ion absorption band (1400–1500 nm) allowed the fundamental resonances to be the reliable signals for sensing.

In the following experiment, we mainly concentrated on the performance of the fundamental mode resonances. The Hi-Bi μ FBG sensor was inserted into a digital heater that could warm the sensor from room temperature to 100 °C. By linear fitting, the measured points, the temperature sensitivities of F-P-1 and F-P-2 could be concluded to 11.6 and 11.5 nm/RIU, respectively, according to Fig. 6b. The difference between the slope rates was relatively small compared to the RI sensitivity divergence. For the microfiber Bragg gratings, the relationship between the Bragg wavelength (λ_B) and the temperature could be theoretically written as

$$\frac{d\lambda_B}{dT} = \lambda_B(\alpha + \beta), \quad (1)$$

where $\alpha = \frac{1}{L} \cdot \frac{dL}{dT}$ is the thermo-expansion coefficient and $\beta = \frac{1}{n_{\text{eff}}} \cdot \frac{dn_{\text{eff}}}{dT}$ is the thermo-optic coefficient, respectively.

For the normal silica-based optical fiber, compared with α of 5×10^{-7} , β (7×10^{-6}) predominated the temperature sensitivity of the fiber Bragg grating. The asymmetrical cross-section of the elliptical microfiber rendered the absolute geometric birefringence rather than the stress-induced birefringence, which was provided by the conventional bow-tie or panda fiber. Therefore, the thermo-optic coefficients were similar between the polarized resonances. In the experiment, the disparity of the temperature sensitivities between F-P-1 and F-P-2 was almost negligible (only 0.1 pm/°C), featuring the characteristics of the geometry-induced polarized resonances and thus facilitating the temperature compensation by logging the dual resonances simultaneously.

Immunosensing

After characterization of the physical measurand sensing of the Hi-Bi μ FBG, we had conducted a further demonstration on the immunosensing capability of the probe. At first, the sensor with the silica surface should be functionalized with the bio-receptors of antibody. The specific detection was realized by the antibody-antigen binding reaction, in which the surface refractive index increased. The Bragg wavelengths of the resonances would also shift accordingly. The correspondence between the Bragg wavelength and the analyte concentration enabled the immunosensing curve,

mediated by the surface refractive index change. For grating the functionalization to the sensor probe, the covalent linking approach was utilized to enable a reliable configuration. The functionalization procedure of the Hi-Bi μ FBG probe was charted in Fig. 7. Note that the Hi-Bi μ FBG probe underwent a 10 min-rinsing of DI water for removing the residual unbonded molecules and stabilized at each end of the procedures.

1. Hydroxylation. The Hi-Bi μ FBG probe was rinsed by the piranha solution (98% sulfuric acid and 30% hydrogen peroxide with the volume ratio of 3:1) for 1 h to endow the silica surface with hydroxyl.
2. Silanization. The probe was immersed into the 5% APTES ethanol solution for 1 h to render the amino-group on the silica surface.
3. Cross-link. The probe was inserted into the 2.5% glutaraldehyde PBS solution for 30 min. The glutaraldehyde would be decorated on the silica surface by use of one of the aldehyde groups that linked the APTES-induced amino-group, remaining another free aldehyde group on standby.
4. Functionalization. The probe was immersed into the human IgG (immunoglobulin G) antibody spiked PBS solution (100 μ g/mL) for 30 min. The amino-group of the human IgG antibody was anchored with the aldehyde group on the fiber surface. A monolayer of IgG antibody was immobilized on the probe.

After functionalization, the fiber probe was characterized using the atom force microscope (AFM) for validating the immobilization of the antibody. As shown in the inset of Fig. 7, functionalized fiber enabled a more significant roughness with a max height of 7 nm in scale. In contrast, the bare fiber had shown a smoother morphology on the surface with a max height of 2 nm. By following the second-order flatten processing, the functionalized fiber presented a surface roughness of 0.961 nm, which was higher than the bare one by three-fold, featuring the successful immobilization of the bio-receptors of antibodies on the surface of the fiber grating probe.

To verify the specific detection of the antigen that matches the bio-receptors using the proposed fiber probe, we prepared three kinds of analytes samples, the 100 μ g/mL of anti-IgG, 10 μ g/mL of anti-IgG, and 100 μ g/mL of Bovine Serum Albumin (BSA), which were all spiked by the PBS buffer.

At first, the wavelength shifts with regard to the specific immuno-binding for the 100 μ g/mL IgG sample were monitored in real-time. The total response time for each detection was 60 min. The detection was repeated three times using the same Hi-Bi μ FBG, which could eliminate the additional error that was caused by exploiting the different fiber

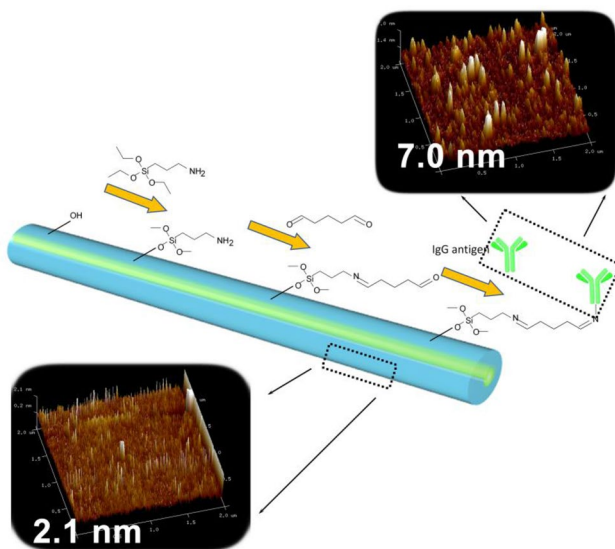


Fig. 7 Scheme of functionalization of the Hi-Bi μ FBG. Insets: comparison between the bare fiber (lower) and functional fiber (upper) using atomic force microscope (AFM)

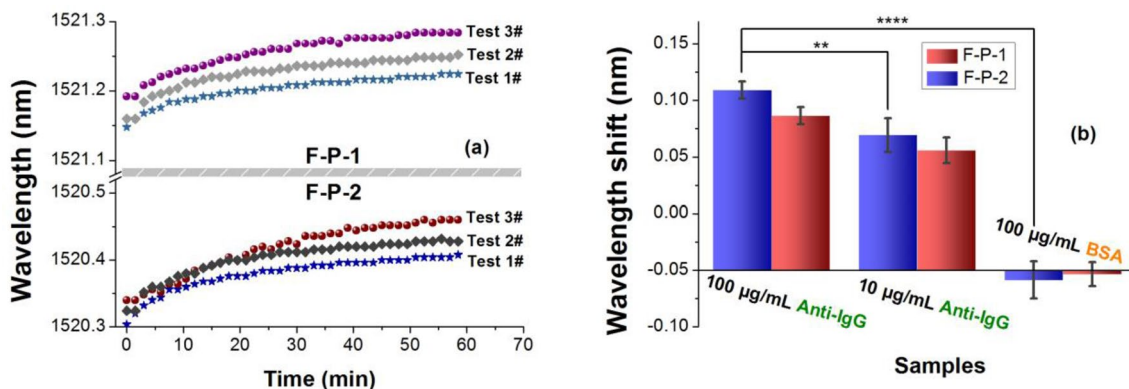


Fig. 8 **a** Kinetics of the resonances in the response of the IgG sample (100 µg/mL); **b** Response of the resonances to the different µg concentrations of IgG samples and non-specific BSA samples (statistical hypothesis t-test, ** $p < 0.05$ and **** $p < 0.001$)

Bragg grating devices. Before each independent test, the Hi-Bi µFBG was rinsed by the piranha solution for 30 min to remove the entire functional layer on the surface, and thus the silica surface of the probe was restored [31, 54]. A new modification process was conducted to refabricate the immunosensor for a new anti-IgG test, following the functionalization procedures ab initio. The time-dependent wavelength shifts of the Hi-Bi µFBG probe corresponding to the 100 µg/mL IgG sample were logged in Fig. 8a. In the three independent tests, the polarized Bragg wavelengths had shown a positive and growing change, indicating the anti-IgG molecules were bond on the probe. However, as shown in Fig. 8b, the F-P-2 resonance exhibited a larger response of 109 ± 8 pm than the F-P-1 resonance of 87 ± 8 pm, correlating well with the difference of the RI sensitivity between the two signals. For the test on the lower concentration of anti-IgG sample (10 µg/mL), the dual resonances presented smaller responses ($69 \text{ pm} \pm 15 \text{ pm}$ for F-P-2 and 56 ± 11 pm for F-P-1) but maintained a similar wavelength difference. By exploiting the one-sample hypothesis t-test, the responses of the sensor regarding the different concentrations of the samples exhibited a good statistical significance (statistical hypothesis: ** $p < 0.05$), indicating the capability of the sensor in calibrating different target samples. Subsequently, the specificity of the sensor was surveyed by immersing the probe into the non-specific biomolecule of BSA samples with 100 µg/mL. The negative results ($-58 \text{ pm} \pm 16 \text{ pm}$ for F-P-2 and -53 ± 10 pm for F-P-1) could be observed, inferring the surface density on the probe was reduced by the exclusion of non-specific BSA. A great statistical significance (statistical hypothesis: **** $p < 0.001$) between the target and control tests could manifest the high specificity of the sensing probe aiming at the anti-IgG. The results derived that the temperature compensated immunosensing could be achieved through monitoring the polarized resonances simultaneously due to the similar temperature responsivity. The sensitivity may be taken as a trade-off using this

method, although, the impact could be limited in dynamic sensing regime [55].

Conclusions

This work reported on an efficient method for fabricating the highly birefringent microfiber Bragg grating and showcased its temperature-compensational biosensing capability. The highly birefringent microfiber was obtained by tapering the elliptical cladding fiber that was ablated by the CO₂ laser from the multimode telecom fiber. The ellipticity of the fiber cladding could be tuned by adjusting the intensity of the CO₂ laser, yielding the correspondent geometric birefringence as a microfiber. The considerably large core region derived by the multimode fiber enabled an efficient inscription of a strong FBG. The Hi-Bi µFBG could compensate for the temperature cross-sensitivity in RI sensing by orchestrating the dual-polarized resonances, in which a 5 nm/RIU difference for RI sensing and a 0.1 pm/°C difference for temperature response were obtained. Higher ordered dual-polarized resonances exhibited not only a larger wavelength difference but also a more significant RI sensitivity difference, revealing the compatibility of the polarized resonances with other schemes, such as mode orders. The Hi-Bi µFBG immunosensor was demonstrated through functionalizing the grating by use of the covalent binding approach. The grating immune probe could significantly respond to the 10 µg/mL of anti-IgG sample with high specificity. Future development should concentrate on: (1) The viability of the ablation power other than 27.5 W and repeatability can be improved by further investigating the processing parameters of the CO₂ laser to facilitate the flexible ellipticity manipulation and the scale-up manufacture. (2) The higher-order mode resonances should be optimally designed in longer wavelength that can be tuned by the size of the microfiber for avoiding the hydroxyl absorption band. Thus, a more

useful signal from an additional degree of freedom can facilitate multi-measurands sensing and improve the sensitivity. (3) Compared with the state-of-the-art fiber-optic immunosensing strategies, which enable the RI sensitivity of ranging from several hundreds to several thousands nm/RIU that render sub $\mu\text{g/mL}$ LOD on IgG/anti-IgG [56–58], the sensitivity (several tens of nm/RIU) and LOD ($\mu\text{g/mL}$) proposed in this work is not the front-runner. The sensitivity improvement method should thus be explored to enable a lower limit of detection on the target biomolecules, such as the optimization of the fiber diameter for improving the RI responsivity and exploiting the Fabry–Perot interferometer and the phase-shifted Bragg gratings for implementing the high-resolution biosensing. This work provides a strategy to solve the problem arising from the temperature cross-sensitivity for the fiber-optic biosensors.

Acknowledgements This work was supported by National Natural Science Foundation of China (61775082, U1701268, 61405074, 61805106), Guangdong Natural Science Foundation (2015A030313324, 2018A030313677), the Local Innovative and Research Teams Project of Guangdong Pearl River Talents Program (2019BT02X105), Youth Top-notch Scientific and Technological Innovation Talent of Guangdong Special Support Plan (2019TQ05X136), and the Fundamental Research Funds for the Central Universities.

Declarations

Conflict of interest On behalf of all authors, the corresponding authors state that there is no conflict of interest.

References

- Caucheteur C, Guo T, Albert J. Review of plasmonic fiber optic biochemical sensors: improving the limit of detection. *Anal Bioanal Chem.* 2015;407:3883.
- Chiavaioli F, Baldini F, Tombelli S, Trono C, Giannetti A. Biosensing with optical fiber gratings. *Nanophotonics.* 2017;6:663.
- Chiavaioli F, Gouveia AJC, Jorge ASP, Baldini F. Towards a uniform metrological assessment of grating-based optical fiber sensors: from refractometers to biosensors. *Biosensors.* 2017;7:23.
- Guo T, González-Vila Á, Loyez M, Caucheteur C. Plasmonic optical fiber-grating immunosensing: a review. *Sensors.* 2017;17:2732.
- Yin M, Gu B, An Q-F, Yang C, Guan YL, Yong K-T. Recent development of fiber-optic chemical sensors and biosensors: mechanisms, materials, micro/nano-fabrications and applications. *Coord Chem Rev.* 2018;376:348.
- Guan B-O, Huang Y. Interface sensitized optical microfiber biosensors. *J Lightwave Technol.* 2019;37:2616.
- Li Y, Xu Z, Tan S, Fang F, Yang L, Yuan B, Sun Q. Recent advances in microfiber sensors for highly sensitive biochemical detection. *J Phys D Appl Phys.* 2019;52:493002.
- Socorro-Lerános AB, Santano D, Del Villar I, Matias IR. Trends in the design of wavelength-based optical fibre biosensors (2008–2018). *Biosens Bioelectron X.* 2019;1:100015.
- Xu Y, Bai P, Zhou X, Akimov Y, Png CE, Ang L-K, Knoll W, Wu L. Optical refractive index sensors with plasmonic and photonic structures: promising and inconvenient truth. *Adv Opt Mater.* 2019;7:1801433.
- Zhao Y, Tong R, Xia F, Peng Y. Current status of optical fiber biosensor based on surface plasmon resonance. *Biosens Bioelectron.* 2019;142:111505.
- Zhang L, Tang Y, Tong L. Micro-/nanofiber optics: merging photonics and material science on nanoscale for advanced sensing technology. *iScience.* 2020;23:100810.
- Zhao Q, Yin M, Zhang AP, Prescher S, Antonietti M, Yuan J. Hierarchically Structured nanoporous poly(ionic liquid) membranes: facile preparation and application in fiber-optic pH sensing. *J Am Chem Soc.* 2013;135:5549.
- Yu C, Wu Y, Liu X, Fu F, Gong Y, Rao Y-J, Chen Y. Miniature fiber-optic NH_3 gas sensor based on Pt nanoparticle-incorporated graphene oxide. *Sens Actuators B Chem.* 2017;244:107.
- Li H, Huang Y, Hou G, Xiao A, Chen P, Liang H, Huang Y, Zhao X, Liang L, Feng X, Guan B-O. Single-molecule detection of biomarker and localized cellular photothermal therapy using an optical microfiber with nanointerface. *Sci Adv.* 2019;5:eaax4659.
- Sun L-P, Huang Y, Huang T, Yuan Z, Lin W, Sun Z, Yang M, Xiao P, Ma J, Wang W, Zhang Y, Liu Z, Guan B-O. Optical microfiber reader for enzyme-linked immunosorbent assay. *Anal Chem.* 2019;91:14141.
- Li Y, Fang F, Yang L, Tan S, Yan Z, Sun Q. In-situ DNA hybridization detection based on a reflective microfiber probe. *Opt Express.* 2020;28:970.
- Guo T, Liu F, Liu Y, Chen N-K, Guan B-O, Albert J. In-situ detection of density alteration in non-physiological cells with polarimetric tilted fiber grating sensors. *Biosens Bioelectron.* 2014;55:452.
- Wu Y, Yao B, Zhang A, Rao Y, Wang Z, Cheng Y, Gong Y, Zhang W, Chen Y, Chiang KS. Graphene-coated microfiber Bragg grating for high-sensitivity gas sensing. *Opt Lett.* 2014;39:1235.
- Yin M-J, Yao M, Gao S, Zhang AP, Tam H-Y, Wai P-KA. Rapid 3D patterning of poly(acrylic acid) ionic hydrogel for miniature pH sensors. *Adv Mater.* 2016;28:1394.
- Liu C, Cai Q, Xu B, Zhu W, Zhang L, Zhao J, Chen X. Graphene oxide functionalized long period grating for ultrasensitive label-free immunosensing. *Biosens Bioelectron.* 2017;94:200.
- Hu D, Xu Z, Long J, Xiao P, Liang L, Sun L, Liang H, Ran Y, Guan B-O. Label-free and reproducible chemical sensor using the vertical-fluid-array induced optical fiber long period grating (VIOLIN). *Sensors.* 2020;20:3415.
- Xiao P, Sun Z, Huang Y, Lin W, Ge Y, Xiao R, Li K, Li Z, Lu H, Yang M, Liang L, Sun L-P, Ran Y, Li J, Guan B-O. Development of an optical microfiber immunosensor for prostate specific antigen analysis using a high-order-diffraction long period grating. *Opt Express.* 2020;28:15783.
- Xu F, Horak P, Brambilla G. Optical microfiber coil resonator refractometric sensor. *Opt Express.* 2007;15:7888.
- Xu Z, Luo Y, Liu D, Shum PP, Sun Q. Sensitivity-controllable refractive index sensor based on reflective θ -shaped microfiber resonator cooperated with Vernier effect. *Sci Rep.* 2017;7:9620.
- Chiavaioli F, Zubiate P, Del Villar I, Zamarreño CR, Giannetti A, Tombelli S, Trono C, Arregui FJ, Matias IR, Baldini F. Femtomolar detection by nanocoated fiber label-free biosensors. *ACS Sens.* 2018;3:936.
- Zubiate P, Urrutia A, Zamarreño CR, Egea-Urra J, Fernández-Irigoyen J, Giannetti A, Baldini F, Díaz S, Matias IR, Arregui FJ, Santamaría E, Chiavaioli F, Del Villar I. Fiber-based early diagnosis of venous thromboembolic disease by label-free D-dimer detection. *Biosens Bioelectron X.* 2019;2:100026.
- Shevchenko Y, Francis TJ, Blair DAD, Walsh R, DeRosa MC, Albert J. In situ biosensing with a surface plasmon resonance fiber grating aptasensor. *Anal Chem.* 2011;83:7027.

28. Guo T, Liu F, Liang X, Qiu X, Huang Y, Xie C, Xu P, Mao W, Guan B-O, Albert J. Highly sensitive detection of urinary protein variations using tilted fiber grating sensors with plasmonic nano-coatings. *Biosens Bioelectron.* 2016;78:221.
29. Zhao J, Cao S, Liao C, Wang Y, Wang G, Xu X, Fu C, Xu G, Lian J, Wang Y. Surface plasmon resonance refractive sensor based on silver-coated side-polished fiber. *Sens Actuators B Chem.* 2016;230:206.
30. Lobry M, Lahem D, Loyez M, Debliquy M, Chah K, David M, Caucheteur C. Non-enzymatic D-glucose plasmonic optical fiber grating biosensor. *Biosens Bioelectron.* 2019;142:111506.
31. Liang L, Jin L, Ran Y, Sun L-P, Guan B-O. Fiber light-coupled optofluidic waveguide (FLOW) immunosensor for highly sensitive detection of p53 protein. *Anal Chem.* 2018;90:10851.
32. Gong C, Gong Y, Yang X, Peng G, Rao Y. Pseudo whispering gallery mode optofluidic lasing based on air-clad optical fiber. *J Lightwave Technol.* 2019;37:2623.
33. Sun L, Huang T, Yuan Z, Yang M, Huang Y, Xiao P, Guan B. Ultrasensitive optofluidic interferometer for online monitoring of photocatalytic reactions. *J Lightwave Technol.* 2019;37:5435.
34. Zhang Z, Pan J, Tang Y, Xu Y, Zhang L, Gong Y, Tong L. Optical micro/nanofibre embedded soft film enables multifunctional flow sensing in microfluidic chips. *Lab Chip.* 2020;20:2572.
35. Fang X, Liao CR, Wang DN. Femtosecond laser fabricated fiber Bragg grating in microfiber for refractive index sensing. *Opt Lett.* 2010;35:1007.
36. Zhang Y, Lin B, Tjin SC, Zhang H, Wang G, Shum P, Zhang X. Refractive index sensing based on higher-order mode reflection of a microfiber Bragg grating. *Opt Express.* 2010;18:26345.
37. Ding M, Zervas MN, Brambilla G. A compact broadband microfiber Bragg grating. *Opt Express.* 2011;19:15621.
38. Liu Y, Meng C, Zhang AP, Xiao Y, Yu H, Tong L. Compact microfiber Bragg gratings with high-index contrast. *Opt Lett.* 2011;36:3115.
39. Ran Y, Tan Y-N, Sun L-P, Gao S, Li J, Jin L, Guan B-O. 193nm excimer laser inscribed Bragg gratings in microfibers for refractive index sensing. *Opt Express.* 2011;19:18577.
40. Kou J-L, Ding M, Feng J, Lu Y-Q, Xu F, Brambilla G. Microfiber-based Bragg gratings for sensing applications: a review. *Sensors.* 2012;12:8861–76.
41. Guan B-O, Li J, Jin L, Ran Y. Fiber Bragg gratings in optical microfibers. *Opt Fiber Technol.* 2013;19:793.
42. Ismael R, Lee T, Ding M, Belal M, Brambilla G. Optical microfiber passive components. *Laser Photonics Rev.* 2013;7:350.
43. Sun D, Ran Y, Wang G. Label-free detection of cancer biomarkers using an in-line taper fiber-optic interferometer and a fiber Bragg grating. *Sensors.* 2017;17:2559.
44. Cao Y, Wang X, Guo T, Ran Y, Feng X, Guan B-O, Yao J. High-resolution and temperature-compensational HER2 antigen detection based on microwave photonic interrogation. *Sens Actuators B Chem.* 2017;245:583.
45. Ran Y, Jin L, Sun LP, Li J, Guan BO. Temperature-compensated refractive-index sensing using a single Bragg grating in an abrupt fiber taper. *IEEE Photonics J.* 2013;5:7100208.
46. Ran Y, Xiao P, Zhang Y, Hu D, Xu Z, Liang L, Guan B-O. A miniature pH probe using functional microfiber Bragg grating. *Optics.* 2020;1:202–12.
47. Sun D, Guo T, Ran Y, Huang Y, Guan B-O. In-situ DNA hybridization detection with a reflective microfiber grating biosensor. *Biosens Bioelectron.* 2014;61:541.
48. Ran Y, Long J, Xu Z, Hu D, Guan B-O. Temperature monitorable refractometer of microfiber Bragg grating using a duet of harmonic resonances. *Opt Lett.* 2019;44:3186.
49. Ran Y, Jin L, Sun L-P, Li J, Guan B-O. Bragg gratings in rectangular microfiber for temperature independent refractive index sensing. *Opt Lett.* 2012;37:2649.
50. Xuan H, Ju J, Jin W. Highly birefringent optical microfibers. *Opt Express.* 2010;18:3828.
51. Ran Y, Jin L, Tan Y, Sun L, Li J, Guan B-O. High-efficiency ultraviolet inscription of Bragg gratings in microfibers. *IEEE Photonics J.* 2012;4:181.
52. Ran Y, Jin L, Gao S, Sun L-P, Huang Y-Y, Li J, Guan B-O. Type IIa Bragg gratings formed in microfibers. *Opt Lett.* 2015;40:3802.
53. Sun L-P, Li J, Gao S, Jin L, Ran Y, Guan B-O. Fabrication of elliptical microfibers with CO₂ laser for high-sensitivity refractive index sensing. *Opt Lett.* 2014;39:3531.
54. Liu T, Liang L-L, Xiao P, Sun L-P, Huang Y-Y, Ran Y, Jin L, Guan B-O. A label-free cardiac biomarker immunosensor based on phase-shifted microfiber Bragg grating. *Biosens Bioelectron.* 2018;100:155.
55. Ran Y, Long J, Xu Z, Yin Y, Hu D, Long X, Zhang Y, Liang L, Liang H, Guan B-O. Harmonic optical microfiber Bragg grating immunosensor for the accelerative test of cardiac biomarker (cTn-I). *Biosens Bioelectron.* 2021;179:113081.
56. Chiavaioli F, Biswas P, Trono C, Bandyopadhyay S, Giannetti A, Tombelli S, Basumallick N, Dasgupta K, Baldini F. Towards sensitive label-free immunosensing by means of turn-around point long period fiber gratings. *Biosens Bioelectron.* 2014;60:305.
57. Cardona-Maya Y, Socorro AB, Del Villar I, Cruz JL, Corres JM, Botero-Cadavid JF. Label-free wavelength and phase detection based SMS fiber immunosensors optimized with cladding etching. *Sens Actuators B Chem.* 2018;265:10.
58. Wang B, Wang Q. Sensitivity-enhanced optical fiber biosensor based on coupling effect between SPR and LSPR. *IEEE Sens J.* 2018;18:8303.